

SegmentDreamer: Towards High-fidelity Text-to-3D Synthesis with Segmented Consistency Trajectory Distillation

Jiahao Zhu¹, Zixuan Chen¹, Guangcong Wang², Xiaohua Xie¹, Yi Zhou³

¹School of Computer Science and Engineering, Sun Yat-sen University, Guangzhou, China

²School of Computing and Information Technology, Great Bay University, Dongguan, China

³Zhongshan School of Medicine, Sun Yat-sen University, Guangzhou, China

{zhujh59,chenzx3}@mail2.sysu.edu.cn, wanggc3@gmail.com, {xiexiaoh6,zhouyi}@mail.sysu.edu.cn



Figure 1. Examples of 3D assets generated by *SegmentDreamer*. Our framework addresses the improper conditional guidance issues of recent Consistency Distillation (CD)-based methods and theoretically provides a significantly tighter upper bound on distillation error, enabling high-fidelity text-to-3D generation within a reasonable timeframe (~32 minutes with classifier-free guidance [9] and ~38 minutes combined with Perp-Neg [1]) on a single A100 GPU through 3D Gaussian Splatting (3DGS). Project Page: <https://zjhJOJO.github.io>

Abstract

Recent advancements in text-to-3D generation improve the visual quality of Score Distillation Sampling (SDS) and its variants by directly connecting Consistency Distillation (CD) to score distillation. However, due to the imbalance between self-consistency and cross-consistency, these CD-based methods inherently suffer from improper conditional guidance, leading to sub-optimal generation results. To address this issue, we present **SegmentDreamer**, a novel framework designed to fully unleash the potential of consistency models for high-fidelity text-to-3D generation. Specifically, we reformulate SDS through the proposed Segmented Consistency Trajectory Distillation (SCTD), effectively mitigating the imbalance issues by explicitly defining the relationship between self- and cross-consistency. Moreover, **SCTD** partitions the Probability Flow Ordinary Differential Equation (PF-ODE) trajectory into multiple sub-trajectories and ensures consistency within each segment, which can theoretically provide a significantly tighter upper bound on distillation error. Additionally, we propose a distillation pipeline for a more swift and stable generation. Extensive experiments demonstrate that our **SegmentDreamer** outperforms state-of-the-art methods in visual quality, enabling high-fidelity 3D asset creation through 3D Gaussian Splatting (3DGS).

1. Introduction

Text-to-3D generation aims to create 3D assets that accurately align with text descriptions. It plays a vital role in various domains such as virtual reality, 3D gaming, and film production. One compelling solution is to directly “distill” 3D assets from 2D text-to-image Diffusion Models (DM) [34] through Score Distillation Sampling (SDS) [31, 46], which leverages pre-trained text-to-image DMs as the 3D priors to guide the optimization of differentiable 3D representations, such as Neural Radiance Fields (NeRF) [29] and 3D Gaussian Splatting (3DGS) [17]. Subsequent research focus on improving the performance of SDS in diversity [11, 43, 47], visual quality [3, 16, 22, 24, 25, 47, 48, 51, 53, 57, 58], and multi-view consistency [5, 10, 12, 35, 37].

Recent methods [22, 48] have improved SDS and its variants by incorporating Consistency Distillation (CD) [18, 40] into their distillation loss. However, due to an imbalance between self-consistency and cross-consistency in their losses, these methods inherently suffer from improper conditional guidance when combined with Classifier-Free Guidance (CFG) for generation, ultimately leading to suboptimal outcomes (see



Figure 2. Visual example of existing CD-based methods: CDS [48], GCS [22], and our *SegmentDreamer* with a Classifier-Free Guidance (CFG) scale of 7.5. As shown, improper conditional guidance leads to suboptimal results. (a) Ineffective guidance produces semantically inconsistent details, while (b) excessive guidance results in overexposure and artifacts. Although (c) Brightness-Equalized Generation (BEG) [22] can mitigate overexposure, artifacts persist. In contrast, our *SegmentDreamer* enhances conditional generation, producing high-fidelity 3D assets.

Figure 2, a detailed explanation is provided in Section 4.1). Additionally, the distillation error upper bound of these methods remains large, limiting their generation quality.

To address the aforementioned limitations, we present a novel framework – *SegmentDreamer*, which aims to fully unleash the potential of consistency models for high-fidelity text-to-3D generation. Specifically, by analyzing existing CD-based methods, we draw inspiration from segmented consistency models [33, 44] to reformulate SDS through the proposed Segmented Consistency Trajectory Distillation (SCTD), which effectively mitigates the imbalance between self-consistency and cross-consistency by explicitly defining their relationship. Moreover, unlike CD-based methods that directly enforce consistency across the entire Probability Flow Ordinary Differential Equation (PF-ODE) trajectory, *SCTD* partitions the PF-ODE trajectory into multiple sub-trajectories, ensuring consistency within each segment. This approach theoretically provides a significantly tighter upper bound on distillation error. In addition, we propose a distillation pipeline for a more swift and stable generation. We also introduce 3DGS as our 3D representation. Extensive experimental results demonstrate that our *SegmentDreamer* outperforms state-of-the-art methods in visual quality. Moreover, the proposed *SCTD* can be seamlessly applied to various 3D generative tasks (*e.g.*, 3D avatar generation, and 3D portrait generation), facilitating the creation of high-fidelity 3D assets.

The main contributions are summarized as follows:

- We present *SegmentDreamer*, a novel framework for high-fidelity text-to-3D generation, which addresses the imbalance issue of existing CD-based methods.
- We reformulate SDS through the proposed *SCTD*,

effectively mitigating the imbalance between self- and cross-consistency. *SCTD* also theoretically provides a significantly tighter upper bound on distillation error. We further propose a distillation pipeline for more swift and stable optimization.

- Experimental results demonstrate that our *SegmentDreamer* outperforms state-of-the-art methods in visual quality, enabling high-fidelity 3D asset generation through 3DGS.

2. Related Work

2.1. Text-to-3D Generation

Creating a 3D object from a given text description is a long-standing challenge in the fields of computer vision and graphics. To achieve this goal, a series of end-to-end text-to-3D pipelines have been proposed [7, 8, 13, 21, 30, 49], but these methods require large-scale labeled 3D datasets for training. To reduce the reliance degree of 3D training data, a compelling solution is to directly “distill” 3D assets from 2D text-to-image Diffusion Models (DM) [34]. A groundbreaking contribution in this domain is DreamFusion [31], which introduced Score Distillation Sampling (SDS) loss to optimize parametric 3D representations. Follow-up works focus on refining and extending SDS in various aspects. For example, several studies [11, 43, 47] improve SDS in diversity through prompting modifications, while [3, 16, 22, 24, 25, 47, 48, 51, 53, 57, 58] enhance the fidelity of the generated 3D objects. Other advancements aim to achieve multi-view consistency [5, 10, 12, 35, 37] and faster generation [42, 52]. Recently, Consistency Distillation (CD) [18, 40] has received widespread attentions as it enables high-quality generation through minimal sampling steps. Inspired by CD, Wu *et al.* [48] and Li *et al.* [22] incorporate CD into their distillation loss, which addresses some limitations brought by SDS. However, these CD-based methods inherently suffer from improper conditional guidance, ultimately leading to sub-optimal results. In this work, we aim to unleash the potential of CD to generate high-fidelity 3D assets, pushing the boundaries of text-to-3D synthesis.

2.2. Differentiable 3D Representations

Neural Radiance Field (NeRF) [29] aims to construct implicit 3D representations using a multi-layer perceptron (MLP), leveraging standard volumetric rendering [14] and alpha compositing techniques [32]. Subsequent research has explored adapting NeRF to various applications, Subsequent research has explored adapting NeRF to various applications, including sparse-view reconstruction [45], anti-aliasing [2], and

medical image super-resolution [4].

3D Gaussian Splatting (3DGS) [17] has emerged as a leading approach for 3D representation, offering rapid optimization and high-speed rendering. Unlike NeRF, 3DGS explicitly models scenes using a set of 3D Gaussians and renders views through splatting [20]. Its versatility has enabled applications across various domains, including avatar generation [36, 55], single-view reconstruction [41], anti-aliasing [54], digital watermarking [6], and SLAM [28, 50].

3. Preliminaries

Diffusion Model (DM) [15, 38, 39] consists of a diffusion process and a denoising process. The diffusion process can be modeled as the solution of an Itô stochastic differential equation (SDE) with the transition kernel $\mathbb{P}(\mathbf{z}_t|\mathbf{z}_0) := \mathcal{N}(\mathbf{z}_t; \alpha_t\mathbf{z}_0, \sigma_t\mathbf{I})$. By reversing the diffusion process, \mathbf{z}_0 can be estimated by solving a Probability Flow Ordinary Differentiable Equation (PF-ODE), which is defined by $d\mathbf{z}_t = [f(t)\mathbf{z}_t - \frac{1}{2}g(t)^2\nabla_{\mathbf{z}_t}\log\mathbb{P}(\mathbf{z}_t)]dt$. A neural network $\epsilon_\phi(\mathbf{z}, t)$ can be trained to approximate the scaled score function $-\sigma_t\nabla_{\mathbf{z}_t}\log\mathbb{P}(\mathbf{z}_t)$, offering an empirical formulation of the PF-ODE: $d\mathbf{z}_t = [f(t)\mathbf{z}_t + \frac{g(t)^2}{2\sigma_t}\epsilon_\phi(\mathbf{z}_t, t)]dt$.

Consistency Model [27, 40] aims to achieve few-step inference by distilling a pre-trained DM ϕ into a student model ϕ' . Given a PF-ODE trajectory $\{\mathbf{z}_t\}_{t\in[0,T]}$ and a condition \mathbf{y} , a consistency model $\mathbf{f}_{\phi'}$ builds the mapping $\mathbf{f}_{\phi'}(\mathbf{z}_t, t, \mathbf{y}) = \mathbf{z}_0$ between any points along this trajectory and the endpoint \mathbf{z}_0 by minimizing the following Consistency Distillation (CD) loss:

$$\mathcal{L}_{\text{CD}} = \mathbb{E}[\lambda(t)\|\mathbf{f}_{\phi'}(\mathbf{z}_t, t), \mathbf{f}_{\phi_s^-}(\hat{\mathbf{z}}_s^\Phi, s)\|_2^2], t > s, \quad (1)$$

where $\mathbf{z}_t = \alpha_t\mathbf{z}_0 + \sigma_t\epsilon$ for $\epsilon \sim \mathcal{N}(\mathbf{0}, \mathbf{I})$ and ϕ_s^- is updated with the exponential moving average [27, 40]. $\hat{\mathbf{z}}_s^\Phi$ can be obtained by:

$$\begin{aligned} \hat{\mathbf{z}}_s^\Phi &= \Phi(\mathbf{z}_t, t, s, \mathbf{y}) \\ &= \mathbf{z}_t + \int_t^s [f(u)\mathbf{z}_u + \frac{g(u)^2}{2\sigma_u}\epsilon_\phi(\mathbf{z}_u, u, \mathbf{y})]du. \end{aligned} \quad (2)$$

The consistency function \mathbf{f}_{ϕ_s} can be parameterized in various ways [27, 40], and the solver $\Phi(\cdot, \cdot, \cdot, \cdot)$ is used to calculate the point at s , which can be implemented using DDIM [38] or DPM-solver [26].

Score Distillation Sampling (SDS) Loss. Given a 3D representation θ that can render a view image $\mathbf{z}_0 := \mathbf{g}(\mathbf{c}, \theta)$ with camera pose \mathbf{c} , SDS distills a 2D DM ϕ to generate a 3D object. by minimizing the following SDS loss *w.r.t.* θ :

$$\mathcal{L}_{\text{SDS}} := \mathbb{E}_{t, \epsilon}[\omega(t)\|\underbrace{\epsilon_\phi(\mathbf{z}_t, t, \mathbf{y}) - \epsilon}_{\text{noise residual}}\|_2^2], \quad (3)$$

where $\mathbf{z}_t = \alpha_t \mathbf{z}_0 + \sigma_t \epsilon$. Poole *et al.* [31] empirically omit the U-Net Jacobian term $\frac{\partial \epsilon_\phi(\mathbf{z}_t, t, \mathbf{y})}{\mathbf{z}_t}$ in gradient calculation for speed-up, leading to low-fidelity results.

4. Our Method

In this section, we first review the mechanism of existing Consistency Distillation (CD)-based methods [22, 48] and reveal that they inherently suffer from improper conditional guidance when combined with Classifier-free Guidance (CFG). Subsequently, we address these limitations by reformulating SDS through the lens of the proposed Segmented Consistency Trajectory Distillation (SCTD). Moreover, building on this insight, we propose the efficient SCTD sampling for high-fidelity text-to-3D generation. We further tailor a distillation pipeline for the proposed SCTD sampling to achieve more swift and stable optimization. Finally, we provide a theoretical proof for our distillation error upper bound. The overall framework of our *SegmentDreamer* is depicted in Fig. 3, with the algorithm detailed in Algorithm 1.

4.1. Reviewing CD-based Losses

The consistency function *w.r.t.* 3D representation θ is parameterized by $\mathbf{F}_\theta(\mathbf{z}_t, t, \mathbf{y}) = \frac{\mathbf{z}_t - \sigma_t \epsilon_\phi(\mathbf{z}_t, t, \mathbf{y})}{\alpha_t}$ [22, 48]. Before proceeding, we clarify two key concepts: self-consistency and cross-consistency. The former ensures that all points on the same ODE trajectory consistently map to their original points, as in consistency models [18, 27, 40]. The latter enforces an alignment between unconditional and conditional ODE trajectories [22]. **Consistency Distillation Sampling (CDS)** loss [48] is defined as

$$\mathcal{L}_{\text{CDS}}(\theta) = \mathbb{E}_{t,s}[c(t) \|\mathbf{F}_\theta(\mathbf{z}_t, t, \mathbf{y}) - \mathbf{F}_\theta(\hat{\mathbf{z}}_s^\Phi, s, \mathbf{y})\|_2^2], \quad (4)$$

where $s < t$, $c(t) = \omega(t) \left(\frac{\alpha_t}{\sigma_t}\right)^2$, and $\hat{\mathbf{z}}_s^\Phi$ is estimated using single-step DDIM sampling. Eq. (4) reveals that CDS prioritizes self-consistency while omitting cross-consistency in its loss function, which can be interpreted as the absence of the ‘‘classifier score’’. As reported in CSD [53], this missing component, crucial for conditional generation, hinders CDS from producing semantically consistent content (see Fig. 5 for details). Moreover, the reliance on \mathbf{F}_θ may introduce a significant distillation error upper bound $\mathcal{O}(\Delta_t)T$, where $\Delta_t = \max |t - s|$. This issue is particularly pronounced in text-to-3D settings due to the typically large $|t - s|$. **Guided Consistency Sampling (GCS)** [22] leverages the DPM-Solver-1 [26] as its consistency function:

$$\mathbf{G}_\theta(\mathbf{z}_t, t, s, \mathbf{y}) = \frac{\alpha_s}{\alpha_t} \mathbf{z}_t - \alpha_s \epsilon_\phi(\mathbf{z}_t, t, \mathbf{y}) \int_{\lambda_t}^{\lambda_s} e^{-\lambda} d\lambda, \quad (5)$$

where $\lambda_t = \ln \frac{\alpha_t}{\sigma_t}$. Based on Eq. (5), GCS proposes a more compact consistency (CC) loss \mathcal{L}_{CC} defined as

$$\mathcal{L}_{\text{CC}}(\theta) = \mathbb{E}_{t,s,e}[\|\mathbf{G}_\theta(\hat{\mathbf{z}}_t^\Phi, t, e, \emptyset) - \mathbf{G}_\theta(\hat{\mathbf{z}}_s^\Phi, s, e, \emptyset)\|_2^2], \quad (6)$$

where $e < s < t$. Moreover, GCS employs a conditional guidance loss \mathcal{L}_{CG} and a pixel-wise constraint \mathcal{L}_{CP} to enforce cross-consistency (see Supp. A for details).

However, GCS loss suffers from improper conditional guidance due to two key issues: (1) \mathbf{G}_θ used to enforce cross-consistency is inherently flawed due to the absence of a target time-step in $\epsilon_\phi(\mathbf{z}_t, t, \mathbf{y})$, as detailed in App. B. (2) GCS employs \mathbf{F}_θ , implemented via one-step DDIM, to enforce cross-consistency throughout the ODE trajectory in both latent and pixel spaces. However, as reported in its paper, it suffers from unstable generation due to the excessive conditional guidance, leading to overexposure and artifacts. Furthermore, this approach results in a less stringent upper bound on the distillation error, expressed as $\mathcal{O}(\Delta_t)(T - e)$, which constrains its generation quality.

Summary: The improper conditional guidance in CDS and GCS arises mainly from an imbalance between self-consistency and cross-consistency. Moreover, the reliance on \mathbf{F}_θ to enforce consistency across the entire trajectory further contributes to this issue.

4.2. Reframing SDS through SCTD

We address the previous limitations by reframing SDS through the lens of SCTD. Specifically, we first define our consistency function as follows: as existing segmented consistency models [33, 44] do, we partition the entire time-step range $[0, T]$ into N_s sub-intervals (*i.e.*, $N_s + 1$ edge points), represented by $\{[s_m, s_{m+1}) | m \in \{0, \dots, N_s - 1\}, s_0 = 0, s_{N_s} = T\}$ (the segmentation strategy will be discussed Sec. 4.3). We define our consistency function \mathbf{G}_θ using Eq. (5), aiming to enforce consistency within each sub-trajectory. *i.e.*, $\mathbf{G}_\theta(\mathbf{z}_t, t, s_m, \mathbf{y}) = \mathbf{G}_\theta(\mathbf{z}_s, s, s_m, \mathbf{y})$ for $s_m \leq s < t \leq s_{m+1}$. For brevity, we abbreviate $\mathbf{G}_\theta(\mathbf{z}_t, t, s_m, \mathbf{y})$ as $\mathbf{G}_\theta^m(\mathbf{z}_t, t, \mathbf{y})$. Notably, our consistency function \mathbf{G}_θ^m avoids the issues inherent in GCS, as analyzed in Sec. 4.1 and Supp. B, since at each training stage, the target time step s_m is always uniquely determined.

When CFG [9] with scale ω is used, the noise residual term in Eq. (3) can be transformed into

$$\hat{\epsilon}_\phi(\mathbf{z}_t, t, \mathbf{y}) - \epsilon = \epsilon_\phi(\mathbf{z}_t, t, \mathbf{y}) - \epsilon + \omega(\epsilon_\phi(\mathbf{z}_t, t, \mathbf{y}) - \epsilon_\phi(\mathbf{z}_t, t, \emptyset)). \quad (7)$$

Based on Eq. (7), \mathcal{L}_{SDS} can be expressed in the form

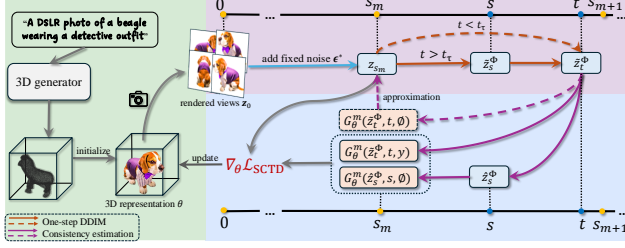


Figure 3. An overview of **SegmentDreamer**: We begin by initializing a 3D representation θ using a 3D generator, such as Point-E [30]. In each iteration, we randomly render a batch of camera views \mathbf{z}_0 from θ and diffuse them into \mathbf{z}_{s_m} with fixed noise ϵ^* . Next, we transform \mathbf{z}_{s_m} into $\hat{\mathbf{z}}_t^\Phi$ using either one-step or two-step unconditional deterministic sampling. During the denoising process, we first estimate $\hat{\mathbf{z}}_s^\Phi$ through one-step conditional deterministic sampling from $\hat{\mathbf{z}}_t^\Phi$. Subsequently, we compute two consistency functions and utilize them to derive the loss $\mathcal{L}_{\text{SCTD}}$, which is ultimately employed to optimize θ .

of SCTD:

$$\mathcal{L}_{\text{SDS}}(\theta) = \mathbb{E}_{t,s}[b(t) \underbrace{\| \mathbf{G}_\theta^m(\hat{\mathbf{z}}_s^\Phi, s, \mathbf{y}) - \mathbf{G}_\theta^m(\mathbf{z}_t, t, \mathbf{y}) \|}_{\text{self-consistency constraint}} + \underbrace{\omega (\mathbf{G}_\theta^m(\mathbf{z}_t, t, \emptyset) - \mathbf{G}_\theta^m(\mathbf{z}_t, t, \mathbf{y})) + \mathbf{z}_{s_m} - \mathbf{G}_\theta^m(\hat{\mathbf{z}}_s^\Phi, s, \mathbf{y})}_{\text{cross-consistency constraint} + \text{generative prior}} \|^2_2]. \quad (8)$$

where $b(t) = \frac{\omega(t)}{(\alpha_{s_m} \int_{\lambda_t}^{\lambda_{s_m}} e^{-\lambda d \lambda})^2}$ and $\hat{\mathbf{z}}_s^\Phi = \Phi(\mathbf{z}_t, t, s, \mathbf{y})$.

The derivation is given in App. C. The first term on the *r.h.s.* of Eq. (8) enforces self-consistency across the conditional denoising sub-trajectory, referred to as the “self-consistency constraint”. The second term enforces cross-consistency between the unconditional and conditional denoising sub-trajectories, termed the “cross-consistency constraint”. The third term adheres to the naming conventions in CSD [53].

As observed, Eq. (8) explicitly defines the relationship between the self-consistency constraint and the cross-consistency constraint, effectively addressing the imbalance problem present in previous CD-based methods [22, 48]. Furthermore, as demonstrated in Sec. 4.3, SCTD provides a tighter upper bound on distillation error, enhancing the upper limit of our algorithm.

4.3. SCTD Sampling

Sampling Design. A natural question arises: according to Eq. (8), does minimizing \mathcal{L}_{SDS} necessarily enforce both self- and cross-consistency? The answer is no. This can be easily understood by noting that one cannot necessarily achieve $x_1 = x_2$ and $y_1 = y_2$ when $\|x_1 - x_2 + \omega(y_1 - y_2)\|_2^2 = 0$. While Eq. (8) provides valuable insights, applying it to text-to-3D tasks re-

Algorithm 1 Text-to-3D Generation via SCTD Loss

- 1: **Initialization:** threshold t_τ , segmentation number N_s , and target prompt \mathbf{y}
- 2: Initialize θ with a pre-trained 3D generator
- 3: **while** θ is not converged **do**
- 4: Sample $\mathbf{z}_0 = \mathbf{g}(\mathbf{c}, \theta)$ and $t \sim \mathcal{U}(0, T)$
- 5: Obtain $s_m = \max\{s_i | s_i \leq t, i = 0, \dots, N_s - 1\}$
- 6: Obtain $\mathbf{z}_{s_m} = \alpha_{s_m} \mathbf{z}_0 + \sigma_{s_m} \epsilon^*$
- 7: Sample $s \sim \mathcal{U}(s_m, t)$
- 8: Predict $\hat{\mathbf{z}}_t^\Phi$ with Eq. (11) and $\hat{\mathbf{z}}_s^\Phi = \Phi(\hat{\mathbf{z}}_t^\Phi, t, s, \mathbf{y})$
- 9: Obtain $\mathbf{G}_\theta^m(\hat{\mathbf{z}}_s^\Phi, s, \emptyset), \mathbf{G}_\theta^m(\hat{\mathbf{z}}_t^\Phi, t, \mathbf{y})$ with Eq. (5)
- 10: Obtain $\nabla_\theta \mathcal{L}_{\text{SCTD}}$ with Eq. (10) and update θ .
- 11: **end while**

mains challenging. To address this, we introduce the following modifications. First, we observe that the condition \mathbf{y} appears in all three loss terms in Eq. (8), which increases computational cost particularly when using Perp-Neg [1] or ControlNet [56]. To mitigate this, we apply an equivalent transformation to it:

$$\mathcal{L}_{\text{SDS}}(\theta) = \mathbb{E}_{t,s}[b(t) \underbrace{\| \mathbf{G}_\theta^m(\hat{\mathbf{z}}_s^\Phi, s, \emptyset) - \mathbf{G}_\theta^m(\mathbf{z}_t, t, \emptyset) \|}_{\text{self-consistency constraint}} + (\omega + 1) \underbrace{\| \mathbf{G}_\theta^m(\mathbf{z}_t, t, \emptyset) - \mathbf{G}_\theta^m(\mathbf{z}_t, t, \mathbf{y}) \|}_{\text{cross-consistency constraint}} + \underbrace{\| \mathbf{z}_{s_m} - \mathbf{G}_\theta^m(\hat{\mathbf{z}}_s^\Phi, s, \emptyset) \|_2^2}_{\text{generative prior}})]. \quad (9)$$

The derivation is given in Supp. D.

We follow the suggestion of CSD [53], omitting the generative prior from Eq. (9). To enforce the self- and cross-consistency, we consider a more strict constraint on Eq. (8), defining our SCTD sampling as follows:

$$\mathcal{L}_{\text{SCTD}}(\theta) = \mathbb{E}_{t,s}[b(t) \underbrace{\| sg(\mathbf{G}_\theta^m(\hat{\mathbf{z}}_s^\Phi, s, \emptyset)) - \mathbf{G}_\theta^m(\hat{\mathbf{z}}_t^\Phi, t, \emptyset) \|_2^2}_{\text{self-consistency constraint}} + \underbrace{\| (\omega + 1) (\mathbf{G}_\theta^m(\hat{\mathbf{z}}_t^\Phi, t, \emptyset) - sg(\mathbf{G}_\theta^m(\hat{\mathbf{z}}_t^\Phi, t, \mathbf{y}))) \|_2^2}_{\text{cross-consistency constraint}})]. \quad (10)$$

where $\hat{\mathbf{z}}_t^\Phi$ is obtained through multi-step deterministic sampling from \mathbf{z}_0 , which is discussed in Sec. 4.4. $\mathbf{z}_{s_m} = \alpha_{s_m} \mathbf{z}_0 + \sigma_{s_m} \epsilon^*$ with ϵ^* fixed for the entire training. $\hat{\mathbf{z}}_s^\Phi = \Phi(\hat{\mathbf{z}}_t^\Phi, t, s, \mathbf{y})$ where Φ is implemented by a first-order ODE solver in this work. $sg(\cdot)$ represents stopping gradient backpropagation.

Trajectory Segmentation Strategy. We propose two heuristic trajectory segmentation strategies: equal segmentation and monotonically increasing segmentation. In the first strategy, the entire time-step range $[0, T]$ is uniformly divided into N_s segments, each with an equal duration, *i.e.*, $s_{m+1} - s_m = \frac{T}{N_s}$. In the second strategy, we adopt a monotonically increasing interval segmentation method, where the N_s intervals satisfy the condition: $s_{m+1} - s_m = t_\tau + \frac{2m(T - N_s t_\tau)}{N_s(N_s - 1)}$, $m \in$

$\{0, \dots, N_s - 1\}$. A comparison of these two strategies is provided in Sec. 6.

4.4. Swift and Stable Optimization Pipeline

In previous work [22, 23, 48], $\tilde{\mathbf{z}}_t^\Phi$ is derived from deterministic sampling with a fixed number of steps, lacking flexibility. In this paper, we adopt the following dynamic adjustment strategy: .

$$\tilde{\mathbf{z}}_t^\Phi = \begin{cases} \Phi(\Phi(\mathbf{z}_{s_m}, s_m, s, \emptyset), s_m, t, \emptyset), & \text{if } t > t_\tau \\ \Phi(\mathbf{z}_{s_m}, s_m, t, \emptyset), & \text{if } t \leq t_\tau \end{cases}, \quad (11)$$

This strategy enable us to make a trade-off between generation quality and optimization speed, as evidenced in Sec. 6.

Consistency function Approximation. For faster optimization, we propose approximating $\mathbf{G}_\theta^m(\tilde{\mathbf{z}}_t^\Phi, t, \emptyset)$ as \mathbf{z}_{s_m} , leveraging the theoretical invertibility of the unconditional PF-ODE trajectory defined in Eq. (11). However, since both Φ and \mathbf{G}_θ^m are both implemented in a first-order ODE solver in this paper, perfect invertibility cannot be guaranteed. Nevertheless, we find that this approximation strategy not only eliminates the need to compute the U-Net Jacobian—reducing computational cost—but also improves optimization stability, as demonstrated in Sec. 6.

4.5. Theoretical Analysis of Distillation Error

We theoretically prove that our SCTD loss leads to a tighter upper bound on the distillation error, explaining why SCTD achieves superior generative results. Specifically, the SDS loss can be reformulated as:

$$\begin{aligned} \mathcal{L}_{\text{SDS}} &= \mathbb{E}_t[\omega(t) \|\epsilon_\phi(\tilde{\mathbf{z}}_t^\Phi, t, \mathbf{y}) - \epsilon^*\|_2^2] \\ &= \mathbb{E}_t[b(t) \|\mathbf{z}_{s_m} - \mathbf{G}_\theta^m(\tilde{\mathbf{z}}_t^\Phi, t, \mathbf{y})\|_2^2]. \end{aligned} \quad (12)$$

Based on Eq. (12), we have the following theorem hold:

Theorem 1. *Given a sub-trajectory $[s_m, s_{m+1}]$, let $\Delta t = \max_{t, s \in (s_m, s_{m+1})} \{|t - s|\}$. We assume \mathbf{G}_θ^m satisfies the Lipschitz condition. If there exists a \mathbf{z}_0 satisfying $\mathbf{G}_\theta^m(\tilde{\mathbf{z}}_t^\Phi, t, \mathbf{y}) = \mathbf{G}_\theta^m(\tilde{\mathbf{z}}_s^\Phi, s, \mathbf{y})$ for $\forall t, s \in [s_m, s_{m+1}]$ and a true image $\mathbf{z}^{\text{data}} \sim \mathbb{P}_{\text{data}}(\mathbf{z})$ corresponding to \mathbf{z}_0 , we have*

$$\sup_{t, s \in [s_m, s_{m+1}]} \|\mathbf{z}_0 - \mathbf{z}^{\text{data}}\| = \mathcal{O}(\Delta t)(s_{m+1} - s_m), \quad (13)$$

Proof. The full proof, inspired by consistency model-related works [22, 27, 44, 48], is provided in App. E. \square

Theorem 1 shows that our SCTD loss achieves an arbitrarily small distillation error when the ODE solver’s step size Δt and the segment length $s_{m+1} - s_m$ are

sufficiently small. By choosing an appropriate segment number N_s , we obtain a tighter error upper bound, improving upon the bound $\mathcal{O}(\Delta t)(T)$ in CDS [48] and $\mathcal{O}(\Delta t)(T - e)$ in GCS [22]. This refinement enables more accurate gradient for optimizing the 3D representation θ , leading to higher-quality generative results.

5. Experiments

5.1. Implementation Details

Our text-to-3D algorithm is implemented in PyTorch and trained on an A100 GPU for 5,000 iterations using the Adam optimizer [19]. We utilize Stable Diffusion 2.1 [34] as our foundational generative model and employ Point-E [30] to initialize 3D Gaussians. Hyperparameters related to 3D Gaussian Splatting (3DGS), such as learning rates and camera poses, are set following the guidelines in previous works [22, 23]. $t \sim \mathcal{U}(20, 500 + t_{\text{warm}})$ where t_{warm} decreases linearly from 480 to 0 during the first 1,500 epochs.

5.2. Text-to-3D Generation

Qualitative Comparison. We present a collection of 3D assets generated by SegmentDreamer from different camera views in Fig. 1. Our algorithm effectively produces high-quality, text-aligned 3D assets. To highlight the superior generative capability of SegmentDreamer, we conduct qualitative experiments comparing it with state-of-the-art methods based on Consistent Distillation (CD)—namely, Consistent3D [48] and Connect3D [22]—as well as Score Distillation (SD)-based methods, including DreamFusion [31] and LucidDreamer [23], as illustrated in Fig. 4. For a fair comparison, all methods use Stable Diffusion 2.1 as the foundational generative model. As shown in Fig. 4, Both DreamFusion and Consistent3D suffer from severe Janus artifacts and fail to generate accurate conditional outputs. LucidDreamer encounters issues with overexposure and ineffective conditional generation. Connect3D performs well in both conditional generation and color rendering; however, its results still contain undesired artifacts, particularly in the tiger and beagle models (see Fig. 4). Moreover, as a 3DGS-based method, it requires over an hour to generate a single 3D asset, limiting its practical usability. In contrast, SegmentDreamer can generate high-quality results within about 32 minutes using CFG [9] and 38 minutes using Perp-Neg [1], proving its efficiency and superiority. More comparison results are shown in our supplementary material.

We also compare our SCTD loss with existing CD-based losses, CDS [48] and GCS [22]. For a fair comparison, we use Stable Diffusion 2.1 as the generative model and keep the random seed, guidance scale, and



Figure 4. Qualitative comparisons with two SD-based methods: DreamFusion [31] and LucidDreamer [23], and two CD-based methods: Consistent3D [48] and ConnectCD [22]. CFG scales are set to 100, 7.5, 20~40, 7.5, 7.5, respectively. Our approach yields high-quality results within the shortest time. Please zoom in for details.

3DGS-related parameters consistent across all methods. As shown in Fig. 5, CDS struggles to provide effective conditional guidance at a normal CFG scale, as also noted in [22]. Even at a higher CFG scale, its results remain unsatisfactory due to the lack of cross-consistency in its distillation loss. GCS, meanwhile, suffers from overexposure and artifacts due to excessive conditional guidance. While it attempts to address this with Brightness-Equalized Generation (BEG), artifacts persist (see Fig. 5, zoom in for details). In contrast, our SCTD mitigates ineffective conditional generation, overexposure, and artifacts, striking a better balance between self-consistency and cross-consistency.

Quantitative Comparison. We assess text alignment and human preference for each text-to-3D method in Tab. 1, where we generate 3D models from 40 prompts selected from the DreamFusion Gallery ¹ and compute the average CLIP Score and ImageReward (IR) score across 120 camera views per model. Following Connect3D, we compute the FID score between 40 objects (each renders 120 views) and 50,000 images generated by Stable Diffusion 2.1. As shown, our method achieves the best text align-



Figure 5. Visual comparisons with CDS [48], GCS [22], and GCS+BEG [22]. Artifacts are marked with red circles.

ment, human preference, and fidelity while requiring the least time, showing its superior performance. The 40 prompts are given in the supplementary material.

User Study. We conduct a user study with 40 volunteers to assess the generation quality for each algorithm. Each volunteer reviews eight groups of five 360-

¹<https://dreamfusion3d.github.io/gallery.html>



Figure 6. Ablation study of the trajectory segmentation strategy with segment number N_s and time threshold t_τ . Prompt: *a DSLR photo of the Imperial State Crown of England.*

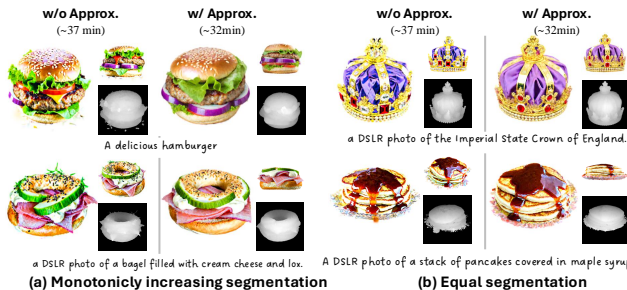


Figure 7. Visual comparison results before and after performing the approximation strategy proposed in Sec. 4.3. “w/ Approx.” and “w/o Approx.” indicate whether the approximation strategy is used or not. The GFG scale is set to 7.5 for all generations.

Table 1. Quantitative comparison using CLIP score, IR score, training time (min), FID score, and three user study questions given by 40 volunteers. **Bold** and underline texts denote the best and second-best performance, respectively.

	CLIP-L \uparrow	IR \uparrow	Time \downarrow	FID \downarrow	Q1 \downarrow	Q2 \downarrow	Q3 \downarrow
DreamFusion[31]	28.47	-0.004	60	140.84	4.73	4.87	4.90
LucidDreamer[23]	29.99	0.006	45	121.80	2.93	2.98	2.93
Consistent3D[48]	30.60	0.004	140	113.61	4.14	3.88	3.93
ConnectCD [22]	30.73	0.018	80	112.61	1.63	1.80	1.93
Ours	30.88	0.020	38	110.45	1.57	1.47	1.33

degree rendered videos and ranks them from the perspective of text alignment (**Q1**), object realism (**Q2**), and object details (**Q3**, *e.g.*, artifact, brightness, Janus problem). To minimize bias, video order is randomized. As shown in Tab. 1, users consistently favor our method across all criteria.

6. Ablation Study

Effect of Trajectory Segmentation Strategy We visualize the effect of different trajectory segmentation strategies applied to our algorithm in Fig. 6. When the segment number N_s and the time threshold t_τ are fixed, we observe that the segmentation strategy has minimal impact on the generated results. This is primarily because the segmentation strategy essentially determines $\sup |t - e|$. However, the timesteps t and s are randomly selected, $|t - s_m|$, $|t - s|$, and $|s - s_m|$ vary randomly during each training iteration, with their values potentially being large or small.

Effect of Segment Number N_s . We visualize the effect of different segment numbers N_s in Fig. 6. As observed, a small N_s , regardless of the segmentation strategy, consistently results in overly smoothed outputs. As N_s increases, the generation quality improves. However, when N_s becomes too large, *e.g.* 10, while more details emerge, the overall model representation becomes vague, which is also mentioned in LucidDreamer [23]. We find that $N_s = 5$ performs well in most cases.

Effect of time threshold t_τ . As shown in Fig. 6, a large t_τ also leads to overly smoothed results for both segmentation strategies. This may be because a limited number of deterministic sampling steps in the diffusion process fails to effectively preserve the information of the initiation point \mathbf{z}_0 , highlighting the necessity of incorporating multi-step deterministic sampling.

Validation of Approximation Strategy. We analyze the impact of replacing $\mathbf{G}_\theta(\tilde{\mathbf{z}}_t^\Phi, t, \mathbf{y})$ with \mathbf{z}_{s_m} in Fig. 7. As shown, $\mathbf{G}_\theta(\tilde{\mathbf{z}}_t^\Phi, t, \mathbf{y})$ introduces slight overexposure and geometry distortion in generation results. In contrast, \mathbf{z}_{s_m} not only produces better generation results but also reduces the training time. This suggests a gap between theory and practice, resembling the omission of U-Net Jacobian in DreamFusion [31].

7. Conclusion

We analyze improper conditional guidance in previous Consistency Distillation methods and identify its root cause as an imbalance between self-consistency and cross-consistency in denoising trajectories. Additionally, we find that large distillation error upper bounds limit generative capability. To address this, we propose the Segmented Consistency Trajectory Distillation loss, which improves conditional guidance and tightens the distillation bound. Experiments show that our SegmentDreamer achieves high-quality generation efficiently, advancing distillation-based text-to-3D methods toward practical use.

Limitation. SegmentDreamer mainly focuses on

single-instance generation and performs suboptimally in multi-instance generation.

Potential Negative Impact. SegmentDreamer focuses on content synthesis, which may be used to create misleading content.

References

- [1] Mohammadreza Armandpour, Ali Sadeghian, Huangjie Zheng, Amir Sadeghian, and Mingyuan Zhou. Re-imagine the negative prompt algorithm: Transform 2d diffusion into 3d, alleviate janus problem and beyond. *arXiv preprint arXiv:2304.04968*, 2023. 1, 5, 6
- [2] Jonathan T Barron, Ben Mildenhall, Matthew Tancik, Peter Hedman, Ricardo Martin-Brualla, and Pratul P Srinivasan. Mip-nerf: A multiscale representation for anti-aliasing neural radiance fields. In *Proceedings of the International Conference on Computer Vision (ICCV)*, pages 5855–5864, 2021. 3
- [3] Rui Chen, Yongwei Chen, Ningxin Jiao, and Kui Jia. Fantasia3d: Disentangling geometry and appearance for high-quality text-to-3d content creation. In *Proceedings of the International Conference on Computer Vision (ICCV)*, pages 22246–22256, 2023. 2, 3
- [4] Zixuan Chen, Lingxiao Yang, Jian-Huang Lai, and Xiaohua Xie. Cunerf: Cube-based neural radiance field for zero-shot medical image arbitrary-scale super resolution. In *Proceedings of the International Conference on Computer Vision (ICCV)*, pages 21185–21195, 2023. 3
- [5] Zilong Chen, Feng Wang, Yikai Wang, and Huaping Liu. Text-to-3d using gaussian splatting. In *Proceedings of the IEEE/CVF Conference on Computer Vision and Pattern Recognition (CVPR)*, pages 21401–21412, 2024. 2, 3
- [6] Zixuan Chen, Guangcong Wang, Jiahao Zhu, Jian-Huang Lai, and Xiaohua Xie. Guardsplat: Efficient and robust watermarking for 3d gaussian splatting. In *Proceedings of the IEEE/CVF Conference on Computer Vision and Pattern Recognition (CVPR)*, 2025. 3
- [7] Jun Gao, Tianchang Shen, Zian Wang, Wenzheng Chen, Kangxue Yin, Daiqing Li, Or Litany, Zan Gojcic, and Sanja Fidler. Get3d: A generative model of high quality 3d textured shapes learned from images. In *Proceedings of the International Conference on Neural Information Processing Systems (NeurIPS)*, pages 31841–31854, 2022. 3
- [8] Anchit Gupta, Wenhan Xiong, Yixin Nie, Ian Jones, and Barlas Öguz. 3dgen: Triplane latent diffusion for textured mesh generation. *arXiv preprint arXiv:2303.05371*, 2023. 3
- [9] Jonathan Ho and Tim Salimans. Classifier-free diffusion guidance. In *Proceedings of the International Conference on Neural Information Processing Systems Workshop (NeurIPS Workshop)*, 2021. 1, 4, 6
- [10] Zhipeng Hu, Minda Zhao, Chaoyi Zhao, Xinyue Liang, Lincheng Li, Zeng Zhao, Changjie Fan, Xiaowei Zhou, and Xin Yu. Efficientdreamer: High-fidelity and robust 3d creation via orthogonal-view diffusion priors. In *Proceedings of the IEEE/CVF Conference on Computer Vision and Pattern Recognition (CVPR)*, pages 4949–4958, 2024. 2, 3
- [11] Yukun Huang, Jianan Wang, Yukai Shi, Boshi Tang, Xianbiao Qi, and Lei Zhang. Dreamtime: An improved optimization strategy for diffusion-guided 3d generation. In *Proceedings of the International Conference on Learning Representations (ICLR)*, 2023. 2, 3
- [12] Chenhan Jiang, Yihan Zeng, Tianyang Hu, Songcun Xu, Wei Zhang, Hang Xu, and Dit-Yan Yeung. Jointdreamer: Ensuring geometry consistency and text congruence in text-to-3d generation via joint score distillation. In *Proceedings of the European Conference on Computer Vision (ECCV)*, pages 439–456. Springer, 2025. 2, 3
- [13] Heewoo Jun and Alex Nichol. Shap-e: Generating conditional 3d implicit functions. *arXiv preprint arXiv:2305.02463*, 2023. 3
- [14] James T Kajiya and Brian P Von Herzen. Ray tracing volume densities. In *ACM SIGGRAPH*, pages 165–174. ACM New York, NY, USA, 1984. 3
- [15] Tero Karras, Miika Aittala, Timo Aila, and Samuli Laine. Elucidating the design space of diffusion-based generative models. In *Proceedings of the International Conference on Neural Information Processing Systems (NeurIPS)*, pages 26565–26577, 2022. 3
- [16] Oren Katzir, Or Patashnik, Daniel Cohen-Or, and Dani Lischinski. Noise-free score distillation. In *Proceedings of the International Conference on Learning Representations (ICLR)*, 2024. 2, 3
- [17] Bernhard Kerbl, Georgios Kopanas, Thomas Leimkühler, and George Drettakis. 3d gaussian splatting for real-time radiance field rendering. *ACM Transactions on Graphics (ACM TOG)*, 42(4):139–1, 2023. 2, 3
- [18] Dongjun Kim, Chieh-Hsin Lai, Wei-Hsiang Liao, Naoki Murata, Yuhta Takida, Toshimitsu Uesaka, Yutong He, Yuki Mitsufuji, and Stefano Ermon. Consistency trajectory models: Learning probability flow ode trajectory of diffusion. In *Proceedings of the International Conference on Learning Representations (ICLR)*, 2024. 2, 3, 4
- [19] Diederik P Kingma and Jimmy Ba. Adam: A method for stochastic optimization. *arXiv preprint arXiv:1412.6980*, 2014. 6
- [20] Georgios Kopanas, Julien Philip, Thomas Leimkühler, and George Drettakis. Point-based neural rendering with per-view optimization. *Computer Graphics Forum (CGF)*, 40(4), 2021. 3
- [21] Muheng Li, Yueqi Duan, Jie Zhou, and Jiwen Lu. Diffusion-sdf: Text-to-shape via voxelized diffusion. In *Proceedings of the IEEE/CVF Conference on Computer Vision and Pattern Recognition (CVPR)*, pages 12642–12651, 2023. 3

- [22] Zongrui Li, Minghui Hu, Qian Zheng, and Xudong Jiang. Connecting consistency distillation to score distillation for text-to-3d generation. In *Proceedings of the European Conference on Computer Vision (ECCV)*, pages 274–291. Springer, 2025. 2, 3, 4, 5, 6, 7, 8, 1
- [23] Yixun Liang, Xin Yang, Jiantao Lin, Haodong Li, Xiaogang Xu, and Yingcong Chen. Luciddreamer: Towards high-fidelity text-to-3d generation via interval score matching. In *Proceedings of the IEEE/CVF Conference on Computer Vision and Pattern Recognition (CVPR)*, pages 6517–6526, 2024. 6, 7, 8, 2, 3
- [24] Chen-Hsuan Lin, Jun Gao, Luming Tang, Towaki Takikawa, Xiao-hui Zeng, Xun Huang, Karsten Kreis, Sanja Fidler, Ming-Yu Liu, and Tsung-Yi Lin. Magic3d: High-resolution text-to-3d content creation. In *Proceedings of the IEEE/CVF Conference on Computer Vision and Pattern Recognition (CVPR)*, pages 300–309, 2023. 2, 3
- [25] Zexiang Liu, Yangguang Li, Youtian Lin, Xin Yu, Sida Peng, Yan-Pei Cao, Xiaojuan Qi, Xiaoshui Huang, Ding Liang, and Wanli Ouyang. Unidream: Unifying diffusion priors for relightable text-to-3d generation. In *Proceedings of the European Conference on Computer Vision (ECCV)*, pages 74–91. Springer, 2025. 2, 3
- [26] Cheng Lu, Yuhao Zhou, Fan Bao, Jianfei Chen, Chongxuan Li, and Jun Zhu. Dpm-solver: A fast ode solver for diffusion probabilistic model sampling in around 10 steps. In *Proceedings of the International Conference on Neural Information Processing Systems (NeurIPS)*, pages 5775–5787, 2022. 3, 4, 1
- [27] Simian Luo, Yiqin Tan, Longbo Huang, Jian Li, and Hang Zhao. Latent consistency models: Synthesizing high-resolution images with few-step inference. *arXiv preprint arXiv:2310.04378*, 2023. 3, 4, 6
- [28] Hidenobu Matsuki, Riku Murai, Paul HJ Kelly, and Andrew J Davison. Gaussian splatting slam. In *Proceedings of the IEEE/CVF Conference on Computer Vision and Pattern Recognition (CVPR)*, pages 18039–18048, 2024. 3
- [29] Ben Mildenhall, Pratul P Srinivasan, Matthew Tancik, Jonathan T Barron, Ravi Ramamoorthi, and Ren Ng. Nerf: Representing scenes as neural radiance fields for view synthesis. *Communications of the ACM*, 65(1): 99–106, 2021. 2, 3
- [30] Alex Nichol, Heewoo Jun, Pratul Dhariwal, Pamela Mishkin, and Mark Chen. Point-e: A system for generating 3d point clouds from complex prompts. *arXiv preprint arXiv:2212.08751*, 2022. 3, 5, 6
- [31] Ben Poole, Ajay Jain, Jonathan T Barron, and Ben Mildenhall. Dreamfusion: Text-to-3d using 2d diffusion. In *Proceedings of the International Conference on Learning Representations (ICLR)*, pages 1–10, 2022. 2, 3, 4, 6, 7, 8
- [32] Thomas Porter and Tom Duff. Compositing digital images. In *Proceedings of the Annual Conference on Computer Graphics and Interactive Techniques*, pages 253–259, 1984. 3
- [33] Yuxi Ren, Xin Xia, Yanzuo Lu, Jiacheng Zhang, Jie Wu, Pan Xie, Xing Wang, and Xuefeng Xiao. Hyper-3d: Trajectory segmented consistency model for efficient image synthesis. In *Proceedings of the International Conference on Neural Information Processing Systems (NeurIPS)*, 2024. 2, 4
- [34] Robin Rombach, Andreas Blattmann, Dominik Lorenz, Patrick Esser, and Björn Ommer. High-resolution image synthesis with latent diffusion models. In *Proceedings of the IEEE/CVF Conference on Computer Vision and Pattern Recognition (CVPR)*, pages 10684–10695, 2022. 2, 3, 6
- [35] Junyoung Seo, Wooseok Jang, Min-Seop Kwak, Hyeonsu Kim, Jaehoon Ko, Junho Kim, Jin-Hwa Kim, Jiyoung Lee, and Seungryong Kim. Let 2d diffusion model know 3d-consistency for robust text-to-3d generation. In *Proceedings of the International Conference on Learning Representations (ICLR)*, 2024. 2, 3
- [36] Zhijing Shao, Zhaolong Wang, Zhuang Li, Duotun Wang, Xiangru Lin, Yu Zhang, Mingming Fan, and Zeyu Wang. Splattingavatar: Realistic real-time human avatars with mesh-embedded gaussian splatting. In *Proceedings of the IEEE/CVF Conference on Computer Vision and Pattern Recognition (CVPR)*, pages 1606–1616, 2024. 3
- [37] Yichun Shi, Peng Wang, Jianglong Ye, Mai Long, Kejie Li, and Xiao Yang. Mvdream: Multi-view diffusion for 3d generation. In *Proceedings of the International Conference on Learning Representations (ICLR)*, 2024. 2, 3
- [38] Jiaming Song, Chenlin Meng, and Stefano Ermon. Denoising diffusion implicit models. In *Proceedings of the International Conference on Learning Representations (ICLR)*, 2021. 3
- [39] Yang Song, Jascha Sohl-Dickstein, Diederik P Kingma, Abhishek Kumar, Stefano Ermon, and Ben Poole. Score-based generative modeling through stochastic differential equations. In *Proceedings of the International Conference on Learning Representations (ICLR)*, 2021. 3
- [40] Yang Song, Pratul Dhariwal, Mark Chen, and Ilya Sutskever. Consistency models. In *Proceedings of the International Conference on Machine Learning (ICML)*, 2023. 2, 3, 4
- [41] Stanislaw Szymanowicz, Christian Rupprecht, and Andrea Vedaldi. Splatter image: Ultra-fast single-view 3d reconstruction. In *Proceedings of the IEEE/CVF Conference on Computer Vision and Pattern Recognition (CVPR)*, pages 10208–10217, 2024. 3
- [42] Jiayang Tang, Jiawei Ren, Hang Zhou, Ziwei Liu, and Gang Zeng. Dreamgaussian: Generative gaussian splatting for efficient 3d content creation. In *Proceedings of the International Conference on Learning Representations (ICLR)*, 2024. 3
- [43] Uy Dieu Tran, Minh Luu, Phong Ha Nguyen, Khoi Nguyen, and Binh-Son Hua. Diverse text-to-3d synthesis with augmented text embedding. In *Proceed-*

- ings of the European Conference on Computer Vision (ECCV)*, pages 217–235. Springer, 2025. 2, 3
- [44] Fu-Yun Wang, Zhaoyang Huang, Alexander William Bergman, Dazhong Shen, Peng Gao, Michael Lingelbach, Keqiang Sun, Weikang Bian, Guanglu Song, Yu Liu, et al. Phased consistency model. In *Proceedings of the International Conference on Neural Information Processing Systems (NeurIPS)*, 2024. 2, 4, 6, 1
- [45] Guangcong Wang, Zhaoxi Chen, Chen Change Loy, and Ziwei Liu. Sparsenerf: Distilling depth ranking for few-shot novel view synthesis. In *Proceedings of the International Conference on Computer Vision (ICCV)*, pages 9065–9076, 2023. 3
- [46] Haochen Wang, Xiaodan Du, Jiahao Li, Raymond A Yeh, and Greg Shakhnarovich. Score jacobian chaining: Lifting pretrained 2d diffusion models for 3d generation. In *Proceedings of the IEEE/CVF Conference on Computer Vision and Pattern Recognition (CVPR)*, pages 12619–12629, 2023. 2
- [47] Zhengyi Wang, Cheng Lu, Yikai Wang, Fan Bao, Chongxuan LI, Hang Su, and Jun Zhu. Prolificdreamer: High-fidelity and diverse text-to-3d generation with variational score distillation. In *Proceedings of the International Conference on Neural Information Processing Systems (NeurIPS)*, pages 8406–8441, 2023. 2, 3
- [48] Zike Wu, Pan Zhou, Xuanyu Yi, Xiaoding Yuan, and Hanwang Zhang. Consistent3d: Towards consistent high-fidelity text-to-3d generation with deterministic sampling prior. In *Proceedings of the IEEE/CVF Conference on Computer Vision and Pattern Recognition (CVPR)*, pages 9892–9902, 2024. 2, 3, 4, 5, 6, 7, 8
- [49] Jianfeng Xiang, Zelong Lv, Sicheng Xu, Yu Deng, Ruicheng Wang, Bowen Zhang, Dong Chen, Xin Tong, and Jiaolong Yang. Structured 3d latents for scalable and versatile 3d generation. *arXiv preprint arXiv:2412.01506*, 2024. 3
- [50] Chi Yan, Delin Qu, Dan Xu, Bin Zhao, Zhigang Wang, Dong Wang, and Xuelong Li. Gs-slam: Dense visual slam with 3d gaussian splatting. In *Proceedings of the IEEE/CVF Conference on Computer Vision and Pattern Recognition (CVPR)*, pages 19595–19604, 2024. 3
- [51] Junliang Ye, Fangfu Liu, Qixiu Li, Zhengyi Wang, Yikai Wang, Xinzhou Wang, Yueqi Duan, and Jun Zhu. Dreamreward: Text-to-3d generation with human preference. In *Proceedings of the European Conference on Computer Vision (ECCV)*, pages 259–276. Springer, 2025. 2, 3
- [52] Taoran Yi, Jiemin Fang, Junjie Wang, Guanjun Wu, Lingxi Xie, Xiaopeng Zhang, Wenyu Liu, Qi Tian, and Xinggang Wang. Gaussiandreamer: Fast generation from text to 3d gaussians by bridging 2d and 3d diffusion models. In *Proceedings of the IEEE/CVF Conference on Computer Vision and Pattern Recognition (CVPR)*, pages 6796–6807, 2024. 3
- [53] Xin Yu, Yuan-Chen Guo, Yangguang Li, Ding Liang, Song-Hai Zhang, and Xiaojuan Qi. Text-to-3d with classifier score distillation. In *Proceedings of the International Conference on Learning Representations (ICLR)*, 2024. 2, 3, 4, 5
- [54] Zehao Yu, Anpei Chen, Binbin Huang, Torsten Sattler, and Andreas Geiger. Mip-splatting: Alias-free 3d gaussian splatting. In *Proceedings of the IEEE/CVF Conference on Computer Vision and Pattern Recognition (CVPR)*, pages 19447–19456, 2024. 3
- [55] Ye Yuan, Xueting Li, Yangyi Huang, Shalini De Mello, Koki Nagano, Jan Kautz, and Umar Iqbal. Gavatar: Animatable 3d gaussian avatars with implicit mesh learning. In *Proceedings of the IEEE/CVF Conference on Computer Vision and Pattern Recognition (CVPR)*, pages 896–905, 2024. 3
- [56] Lvmin Zhang, Anyi Rao, and Maneesh Agrawala. Adding conditional control to text-to-image diffusion models. In *Proceedings of the International Conference on Computer Vision (ICCV)*, pages 3836–3847, 2023. 5
- [57] Junzhe Zhu, Peiye Zhuang, and Sanmi Koyejo. Hifa: High-fidelity text-to-3d generation with advanced diffusion guidance. In *Proceedings of the International Conference on Learning Representations (ICLR)*, 2024. 2, 3
- [58] Wenjie Zhuo, Fan Ma, Hehe Fan, and Yi Yang. Vividreamer: Invariant score distillation for hyper-realistic text-to-3d generation. In *Proceedings of the European Conference on Computer Vision (ECCV)*, pages 122–139. Springer, 2025. 2, 3

SegmentDreamer: Towards High-fidelity Text-to-3D Synthesis with Segmented Consistency Trajectory Distillation

Supplementary Material

To provide proofs of SegmenDreamer and visual comparisons of state-of-the-arts, this supplementary material includes the following contents:

- Section A: Guided Consistency Sampling Loss
- Section B: Flaws in the Consistency Function of Guided Consistency Sampling
- Section C: How to Connect SCTD with SDS
- Section D: Computation Reduction Trick
- Section E: Proof of Upper Bound of Distillation Error
- Section F: Visual comparisons of State-of-the-art
- Section G: Limitation and Potential Negative Impacts

A. Guided Consistency Sampling Loss

The Guided Consistency Sampling (GCS) loss [22] is composed of a compact consistency loss \mathcal{L}_{CC} , a conditional guidance loss \mathcal{L}_{CG} , and a pixel-wise constraint loss \mathcal{L}_{CP} , which are defined by

$$\begin{aligned}\mathcal{L}_{CC}(\theta) &= \mathbb{E}[\|\mathbf{G}_\theta(\hat{\mathbf{z}}_t^\Phi, t, e, \emptyset) - \mathbf{G}_\theta(\hat{\mathbf{z}}_s^\Phi, s, e, \emptyset)\|_2^2], \\ \mathcal{L}_{CG}(\theta) &= \mathbb{E}[\|\mathbf{F}_\theta(\mathbf{z}_e, e, \emptyset) - \mathbf{F}_\theta(\mathbf{G}_\theta(\hat{\mathbf{z}}_t^\Phi, t, e, \mathbf{y}), e, \emptyset)\|_2^2], \\ \mathcal{L}_{CP}(\theta) &= \mathbb{E}[\|D(\mathbf{F}_\theta(\mathbf{z}_e, e, \emptyset)) - D(\mathbf{F}_\theta(\mathbf{G}_\theta(\hat{\mathbf{z}}_t^\Phi, t, e, \mathbf{y}), e, \emptyset))\|_2^2],\end{aligned}\quad (14)$$

where $e < s < t$, $\hat{\mathbf{z}}_t^\Phi$ is estimated by the following trajectory: $\mathbf{z}_e = \alpha_t \mathbf{z}_0 + \sigma_t \epsilon^* \rightarrow \hat{\mathbf{z}}_s^\Phi = \Phi(\mathbf{z}_e, e, s, \emptyset) \rightarrow \hat{\mathbf{z}}_t^\Phi = \Phi(\hat{\mathbf{z}}_s^\Phi, s, t, \emptyset)$, $\hat{\mathbf{z}}_s^\Phi = \Phi(\hat{\mathbf{z}}_t^\Phi, t, s, \mathbf{y})$, and D denotes the VAE decoder.

B. Flaws in the Consistency Function of Guided Consistency Sampling

As we know, given a well-trained diffusion model ϕ , there exists an exact solution from timestep t to e [26]:

$$\mathbf{G}(\mathbf{z}_t, t, e, \mathbf{y}) = \frac{\alpha_e}{\alpha_t} \mathbf{z}_t + \alpha_s \int_{\lambda_t}^{\lambda_e} e^{-\lambda} \epsilon_\phi(\mathbf{z}_{t_\lambda(\lambda)}, t_\lambda(\lambda), \mathbf{y}) d\lambda, \quad (15)$$

where $\lambda_t = \ln \frac{\alpha_t}{\sigma_t}$ and t_λ denotes the inverse function of λ_t . Inspired by [44], we find Eq. (6) suggests that GCS aims to optimize a 3D representation θ such that $\mathbf{G}_\theta(\mathbf{z}_t, t, e, \emptyset) = \mathbf{G}_\theta(\hat{\mathbf{z}}_s^\Phi, s, e, \emptyset)$ for $\forall t, s, e \in [0, T]$ where $t > s > e$. This implies $\epsilon_\phi(\mathbf{z}_t, t, \mathbf{y})$, as defined in Eq. (5), is not an approximation but an exact solution learning related to the 3D representation θ ,

i.e., $\epsilon_\phi(\mathbf{z}_t, t, \mathbf{y}) = \frac{\int_{\lambda_t}^{\lambda_e} e^{-\lambda} \epsilon_\phi(\mathbf{z}_{t_\lambda(\lambda)}, t_\lambda(\lambda), \mathbf{y}) d\lambda}{\int_{\lambda_t}^{\lambda_e} e^{-\lambda} d\lambda}$. However,

dropping the target timestep e in $\epsilon_\phi(\mathbf{z}_t, t, \mathbf{y})$, as GCS does, is problematic. Suppose we predict both \mathbf{z}_e and $\mathbf{z}_{e'}$ from \mathbf{z}_t where $t > e' > e$, we must have

$$\begin{aligned}\epsilon_\phi(\mathbf{z}_t, t, \mathbf{y}) &= \frac{\int_{\lambda_t}^{\lambda_{e'}} e^{-\lambda} \epsilon_\phi(\mathbf{z}_{t_\lambda(\lambda)}, t_\lambda(\lambda), \mathbf{y}) d\lambda}{\int_{\lambda_t}^{\lambda_{e'}} e^{-\lambda} d\lambda} \\ \epsilon_\phi(\mathbf{z}_t, t, \mathbf{y}) &= \frac{\int_{\lambda_t}^{\lambda_e} e^{-\lambda} \epsilon_\phi(\mathbf{z}_{t_\lambda(\lambda)}, t_\lambda(\lambda), \mathbf{y}) d\lambda}{\int_{\lambda_t}^{\lambda_e} e^{-\lambda} d\lambda}.\end{aligned}\quad (16)$$

Clearly, without the target timestep in $\epsilon_\phi(\mathbf{z}_t, t, \mathbf{y})$, optimizing a 3D representation θ to satisfy both conditions in Eq. (16) for all intervals $[e, t]$ is invalid. For GCS, as the number of training steps increases, the above unreasonable phenomena occur frequently, potentially resulting in poor distillation results.

C. How to Connect SCTD with SDS?

As described in Sec. 4.3, given any subtrajectory $[s_m, s_{m+1}]$, $\mathbf{G}_\theta(\mathbf{z}_t, t, s_m, \mathbf{y}) := \mathbf{G}_\theta^m(\mathbf{z}_t, t, \mathbf{y}) = \frac{\alpha_{s_m}}{\alpha_t} \mathbf{z}_t - \alpha_{s_m} \epsilon_\phi(\mathbf{z}_t, t, \mathbf{y}) \int_{\lambda_t}^{\lambda_{s_m}} e^{-\lambda} d\lambda$. Then, we have

$$\epsilon_\phi(\mathbf{z}_t, t, \mathbf{y}) = \frac{\mathbf{G}_\theta^m(\mathbf{z}_t, t, \mathbf{y}) - \frac{\alpha_{s_m}}{\alpha_t} \mathbf{z}_t}{\alpha_{s_m} \int_{\lambda_t}^{\lambda_{s_m}} e^{-\lambda} d\lambda}, \quad (17)$$

where $\mathbf{z}_t = \alpha_t \mathbf{z}_0 + \sigma_t \epsilon$. In this case, \mathbf{y} can represent any prompt embedding, including \emptyset . According to Eq. (7), \mathcal{L}_{SDS} can be further transformed into:

$$\begin{aligned}\hat{\epsilon}_\phi(\mathbf{z}_t, t, \mathbf{y}) - \epsilon &= \epsilon_\phi(\mathbf{z}_t, t, \mathbf{y}) - \epsilon - \mathbf{G}_\theta^m(\hat{\mathbf{z}}_s^\Phi, s, \mathbf{y}) + \mathbf{G}_\theta^m(\hat{\mathbf{z}}_s^\Phi, s, \mathbf{y}) \\ &\quad + \omega(\epsilon_\phi(\mathbf{z}_t, t, \mathbf{y}) - \epsilon_\phi(\mathbf{z}_t, t, \emptyset)),\end{aligned}\quad (18)$$

where $\hat{\mathbf{z}}_s^\Phi = \Phi(\mathbf{z}_t, t, s, \mathbf{y})$. By substituting Eq. (17) into Eq. (18), we obtain

$$\begin{aligned}\mathcal{L}_{SDS}(\theta) &= \mathbb{E}_t[b(t) \|\mathbf{G}_\theta^m(\hat{\mathbf{z}}_s^\Phi, s, \mathbf{y}) - \mathbf{G}_\theta^m(\mathbf{z}_t, t, \mathbf{y}) \\ &\quad + \omega(\mathbf{G}_\theta^m(\mathbf{z}_t, t, \emptyset) - \mathbf{G}_\theta^m(\mathbf{z}_t, t, \mathbf{y})) - \mathbf{G}_\theta^m(\hat{\mathbf{z}}_s^\Phi, s, \mathbf{y})\|_2^2] \\ &\quad + \frac{\alpha_{s_m}}{\alpha_t} \mathbf{z}_t - \alpha_{s_m} \int_{\lambda_t}^{\lambda_{s_m}} e^{-\lambda} d\lambda \epsilon\|_2^2,\end{aligned}\quad (19)$$

where $b(t) = \frac{\omega(t)}{(\alpha_{s_m} \int_{\lambda_t}^{\lambda_{s_m}} e^{-\lambda} d\lambda)^2}$. Furthermore,

$$\begin{aligned} & \frac{\alpha_{s_m} \mathbf{z}_t - \alpha_{s_m} \int_{\lambda_t}^{\lambda_{s_m}} e^{-\lambda} d\lambda \epsilon}{\alpha_t} \\ &= \frac{\alpha_{s_m}}{\alpha_t} (\alpha_t \mathbf{z}_0^c + \sigma_t \epsilon) + \alpha_{s_m} (e^{\lambda_{s_m} - \lambda_t} - 1) \epsilon \\ &= \alpha_{s_m} \mathbf{z}_0 + \sigma_{s_m} \epsilon \\ &= \mathbf{z}_{s_m} \end{aligned} \quad (20)$$

Substituting Eq. (20) into Eq. (19), we can obtain Eq. (8). Proof is completed.

D. Computation Reduction Trick

Eq. (7) can be transformed into

$$\begin{aligned} \hat{\epsilon}_\phi(\mathbf{z}_t, t, \mathbf{y}) - \epsilon &= \epsilon_\phi(\mathbf{z}_t, t, \mathbf{y}) - \epsilon + \omega(\epsilon_\phi(\mathbf{z}_t, t, \mathbf{y}) - \epsilon_\phi(\mathbf{z}_t, t, \emptyset)) \\ &= \epsilon_\phi(\mathbf{z}_t, t, \emptyset) - \epsilon + (\omega + 1)(\epsilon_\phi(\mathbf{z}_t, t, \mathbf{y}) - \epsilon_\phi(\mathbf{z}_t, t, \emptyset)) \end{aligned} \quad (21)$$

Based on Eq. (21), we can readily derive Eq. (9) by following the procedure described in App. C.

E. Proof of Upper Bound of Distillation Error

Before proving Theorem 1, we first give the following lemma:

Lemma 1. *Given a sub-trajectory $[s_m, s_{m+1}]$, let $\Delta t = \max_{t, s \in [s_m, s_{m+1}]} \{t - s\}$. We assume \mathbf{G}_θ^m satisfies the Lipschitz condition and the ODE solver has local error uniformly bounded by $O(t - s)^{p+1}$ with $p \geq 1$. If $\mathbf{G}_\theta^m(\tilde{\mathbf{z}}_t^\Phi, t, \emptyset) = \mathbf{G}_\theta^m(\hat{\mathbf{z}}_s^\Phi, s, \emptyset)$ for $\forall t, s \in [s_m, s_{m+1}]$, we have*

$$\begin{aligned} & \sup_{t, s \in [s_m, s_{m+1}]} \|\mathbf{G}_\theta^m(\tilde{\mathbf{z}}_t^\Phi, t, \mathbf{y}) - \Phi(\tilde{\mathbf{z}}_t^\Phi, t, s_m, \mathbf{y})\| \\ &= O((\Delta t)^p)(s_{m+1} - s_m). \end{aligned} \quad (22)$$

Proof. The proof is based on [22, 40, 44, 48]. Let

$$\mathbf{e}_{n-1} := \mathbf{G}_\theta^m(\tilde{\mathbf{z}}_s^\Phi, s, \mathbf{y}) - \Phi(\tilde{\mathbf{z}}_s^\Phi, s, s_m, \mathbf{y}), \quad (23)$$

where $\tilde{\mathbf{z}}_s^\Phi = \Phi(\mathbf{z}_{s_m}^c, s_m, s, \mathbf{y})$. According to the condition, we have

$$\begin{aligned} \mathbf{e}_n &= \mathbf{G}_\theta^m(\tilde{\mathbf{z}}_t^\Phi, t, \mathbf{y}) - \Phi(\tilde{\mathbf{z}}_t^\Phi, t, s_m, \mathbf{y}) \\ &= \mathbf{G}_\theta^m(\hat{\mathbf{z}}_s^\Phi, s, \mathbf{y}) - \mathbf{G}_\theta^m(\tilde{\mathbf{z}}_s^\Phi, s, \mathbf{y}) \\ &+ \mathbf{G}_\theta^m(\tilde{\mathbf{z}}_s^\Phi, s, \mathbf{y}) - \Phi(\tilde{\mathbf{z}}_s^\Phi, s, s_m, \mathbf{y}) \\ &= \mathbf{G}_\theta^m(\hat{\mathbf{z}}_s^\Phi, s, \mathbf{y}) - \mathbf{G}_\theta^m(\tilde{\mathbf{z}}_s^\Phi, s, \mathbf{y}) + \mathbf{e}_{n-1}, \end{aligned} \quad (24)$$

Provided that \mathbf{G}_θ^m satisfies L -Lipschitz condition, we

have

$$\begin{aligned} \|\mathbf{e}_n\| &= \|\mathbf{e}_{n-1} + \mathbf{G}_\theta^m(\hat{\mathbf{z}}_s^\Phi, s, \mathbf{y}) - \mathbf{G}_\theta^m(\tilde{\mathbf{z}}_s^\Phi, s, \mathbf{y})\| \\ &\leq \|\mathbf{e}_{n-1}\| + \|\mathbf{G}_\theta^m(\hat{\mathbf{z}}_s^\Phi, s, \mathbf{y}) - \mathbf{G}_\theta^m(\tilde{\mathbf{z}}_s^\Phi, s, \mathbf{y})\| \\ &\leq \mathbf{e}_{n-1} + L \|\hat{\mathbf{z}}_s^\Phi - \tilde{\mathbf{z}}_s^\Phi\| \\ &\leq \mathbf{e}_{n-1} + L \cdot O((t - s)^{p+1}) \\ &\leq \mathbf{e}_{n-1} + L(t - s) \cdot O((\Delta t)^p). \end{aligned} \quad (25)$$

Besides, according to the boundray condition,

$$\begin{aligned} \mathbf{e}_{s_m} &= \mathbf{G}_\theta^m(\hat{\mathbf{z}}_{s_m}^\Phi, s_m, \mathbf{y}) - \Phi(\tilde{\mathbf{z}}_{s_m}^\Phi, s_m, s_m, \mathbf{y}) \\ &= \hat{\mathbf{z}}_{s_m}^\Phi - \tilde{\mathbf{z}}_{s_m}^\Phi = \mathbf{z}_{s_m}^c - \mathbf{z}_{s_m}^c = 0, \end{aligned} \quad (26)$$

Therefore,

$$\begin{aligned} \|\mathbf{e}_n\| &\leq \|\mathbf{e}_{s_m}\| + L \sum_{t_i, t_{i-1} \in [s_m, s_{m+1}]} (t_i - t_{i-1}) O((\Delta t)^p) \\ &= O((\Delta t)^p) \cdot (s_{m+1} - s_m). \end{aligned} \quad (27)$$

The proof is completed. \square

According to Eq. (12), one can ideally optimize a 3D model θ such that $\mathbf{z}_{s_m} = \mathbf{G}_\theta^m(\tilde{\mathbf{z}}_t^\Phi, t, \mathbf{y})$. In this case, we have $\Phi(\tilde{\mathbf{z}}_s^\Phi, s, s_m, \mathbf{y}) = \mathbf{z}_{s_m}^{data}$, where $\mathbf{z}_{s_m}^{data} = \alpha_{s_m} \mathbf{z}^{data} + \sigma_{s_m} \epsilon^*$. Based on this, we have

$$\|\mathbf{G}_\theta^m(\tilde{\mathbf{z}}_t^\Phi, t, \mathbf{y}) - \Phi(\tilde{\mathbf{z}}_t^\Phi, t, s_m, \mathbf{y})\| = \|\mathbf{z}_{s_m} - \mathbf{z}_{s_m}^{data}\| = \|\mathbf{z}_0 - \mathbf{z}^{data}\|. \quad (28)$$

Since we use a first-order ODE solver to implement Φ , we have

$$\sup_{t, s \in [s_m, s_{m+1}]} \|\mathbf{z}_0 - \mathbf{z}^{data}\| = \mathcal{O}(\Delta t)(s_{m+1} - s_m). \quad (29)$$

The proof is completed.

F. Visual comparisons of State-of-the-arts

We also provide visual comparisons of State-of-the-arts, as shown in Fig. 8. We provide additional qualitative comparisons with DreamFusion [31], LucidDreamer [23], Consistent3D [48], and ConnectCD [22]. CFG scales are set to 100, 7.5, 20~40, 7.5, 7.5, respectively. Our approach yields results with high quality within the shortest time. In Table 2, we provide the detailed prompts of examples.

G. Limitation and Potential Negative Impact

Limitation. SegmentDreamer is primarily designed for single-instance generation and performs suboptimally in multi-instance generation.

Potential Negative Impact. SegmentDreamer focuses on content synthesis, which could potentially be misused to create misleading or deceptive content.



Figure 8. Additional qualitative comparisons with DreamFusion [31], LucidDreamer [23], Consistent3D [48], and ConnectCD [22]. CFG scales are set to 100, 7.5, 20~40, 7.5, 7.5, respectively. Our approach yields results with high quality within the shortest time. Please zoom in for details.

Table 2. Prompt of examples.

	Prompt
1	A cat with a mullet
2	A pig wearing a backpack
3	A DSLR photo of an origami crane
4	A photo of a mouse playing the tuba
5	An orange road bike
6	A ripe strawberry
7	A DSLR photo of the Imperial State Crown of England
8	A photo of a wizard raccoon casting a spell
9	A DSLR photo of a corgi wearing a top hat
10	A rabbit, animated movie character, high-detail 3D model
11	A panda rowing a boat
12	A highly detailed sand castle
13	A DSLR photo of a chimpanzee dressed like Henry VIII king of England
14	A photo of a skiing penguin wearing a puffy jacket, highly realistic DSLR photo
15	A blue poison-dart frog sitting on a water lily
16	A DSLR photo of a bear dressed in medieval armor
17	A DSLR photo of a squirrel dressed like a clown
18	A plush toy of a corgi nurse
19	A humanoid robot playing the violin
20	A DSLR photo of a bear dressed as a lumberjack
21	A blue motorcycle
22	Michelangelo style statue of an astronaut
23	A DSLR photo of a chow chow puppy
24	A DSLR photo of cats wearing eyeglasses
25	A red panda
26	A DSLR photo of an elephant skull
27	An amigurumi bulldozer
28	A typewriter
29	A red-eyed tree frog, low poly
30	A DSLR photo of a chimpanzee wearing headphones
31	A robot made out of vegetables
32	A DSLR photo of a red rotary telephone
33	A DSLR photo of a blue lobster
34	A DSLR photo of a squirrel flying a biplane
35	A DSLR photo of a baby dragon hatching out of a stone egg
36	A DSLR photo of a bear dancing ballet
37	A plate of delicious tacos
38	A DSLR photo of a car made out of cheese
39	A yellow school bus
40	A DSLR photo of a shiny beetle